Innovative Nanoimprint Tools for Optoelectronic Applications

May 1, 2002

Sponsored by

Defense Advanced Research Projects Agency (DOD)

ARPA Order K475/39

Issued by US Army Aviation and Missile Command Under

Contract No. DAAH01-02-C-R067

Innovative Nanoimprint Tools for Optoelectronic Applications

May 1, 2002

Sponsored by
Defense Advanced Research Projects Agency (DOD)
(Controlling DARPA Office)

ARPA Order K475/39

Issued by US Army Aviation and Missile Command Under
Contract No. DAAH01-02-C-R

Molecular Imprints, Inc.

PI: Dr. Byung-Jin Choi

1807-C. W Braker Lane
Austin, TX 78758
(512) 339-7760
(512) 789-7845
jin@militho.com

Contract period: 24OCT01 – 24APR02
Reporting period: 24OCT01– 24APR02

REPORT DOCUMENTATION PAGE

1. AGENCY USE ONLY (Leave blank)	2. REPORT DATE	3. REPORT TYPE AND DATES COVERED
	May 01	Final Report (24Oct01-24Apr02)

4. TITLE AND SUBTITLE

Innovative Nanoimprint Tools for Optoelectronic Applications

5. FUNDING NUMBERS

DAAH01-02-C-R

6. AUTHOR(S)

Dr. Byung Jin Choi

7. PERFORMING ORGANIZATION NAME(S) AND ADDRESS(ES)

Molecular Imprints, Inc.
P.O. Box 81485
Austin, TX 78708-1485

8. PERFORMING ORGANIZATION REPORT NUMBER

9. SPONSORING/ MONITORING AGENCY NAME(S) AND ADDRESS(ES)

US Army Aviation & Missile Command
AMSAM-AC-RD-A
Tandy Lane (256)842-0744
Redstone Arsenal AL 35898-5280

10. SPONSORING/MONITORING

11. SUPPLEMENTARY NOTES

12a. DISTRIBUTION/AVAILABILITY STATEMENT

Approved for public release; distribution is unlimited.

12b. DISTRIBUTION CODE

13. ABSTRACT (Maximum 200 words)

This project addresses a low pressure, room-temperature nano imprint lithography that uses low viscosity UV curable imprint liquids. As compared to Si wafers, compound semiconductor wafers are known to be more fragile and prone to breakage under localized stresses. Further, the flatness and parallelism for this type of wafers are known to be not as good as those of Si wafers. During imprinting processes, a pushing force occurs when a master mold contacts the wafer via a fluid layer between them and a pulling force applies to the wafer when they separate after the fluid layer is UV cured. Excessive deformation and local stresses can cause either a mechanical failure of the wafers or undesirable imprint layers. During the reported period, imprints were performed on 2" GaAs and 2" InP wafers. Even though the imprinting and separation can induce large forces and deformations to the wafers, they do not appear to cause local stresses to the wafers. However, when there is a particle that can cause a locally concentrated stress in the wafer, wafer failures occurred in the form of crack propagation and breakage failure. In order to avoid the local stress and large deformation to the wafers, fine-grooved wafer chucks were designed and prototyped. Force estimations based on a Newtonian fluid model provided the force-time-thickness relationship of the imprint layer. The thickness variation of the imprinted layer on compound semiconductor wafers was measured. Three potential solutions to handle the excessive surface variation are suggested as future work.

14. SUBJECT TERMS		15. NUMBER OF PAGES
Nano Imprint Lithography	Compound Semiconductor Wafers	28
Wafer Chuck Design	System Design	16. PRICE CODE

17. SECURITY CLASSIFICATION OF REPORT	18. SECURITY CLASSIFICATION	19. SECURITY CLASSIFICATION OF ABSTRACT	20. LIMITATION OF ABSTRACT
UNCLASSIFIED	UNCLASSIFIED	UNCLASSIFIED	UL

Contents

Abstract

This project addresses a low pressure, room-temperature nano imprint lithography that uses low viscosity UV curable imprint liquids. As compared to Si wafers, compound semiconductor wafers are known to be more fragile and prone to breakage under localized stresses. Further, the flatness and parallelism for this type of wafers are known to be not as good as those of Si wafers. During imprinting processes, a pushing force occurs when a master mold contacts the wafer via a fluid layer between them and a pulling force applies to the wafer when they separate after the fluid layer is UV cured. Excessive deformation and local stresses can cause either a mechanical failure of the wafers or undesirable imprint layers. During the reported period, imprints were performed on 2" GaAs and 2" InP wafers. Even though the imprinting and separation can induce large forces and deformations to the wafers, they do not appear to cause local stresses to the wafers. However, when there is a particle that can cause a locally concentrated stress in the wafer, wafer failures occurred in the form of crack propagation and breakage failure. In order to avoid the local stress and large deformation to the wafers, fine-grooved wafer chucks were designed and prototyped. Force estimations based on a Newtonian fluid model provided the force-time-thickness relationship of the imprint layer. The thickness variation of the imprinted layer on compound semiconductor wafers was measured. Three potential solutions to handle the excessive surface variation are suggested as future work.

List of Figures

Summary

Using S-FIL process, both imprinting and separation have been performed on 2" GaAs and InP wafers. It was found that it is to avoid any localized stress in compound semiconductor wafers during imprinting steps particularly due to backside particles contamination. Various wafer chuck designs were investigated to provide proper support with minimal backside surface contact. Even though imprints with the new wafer chucks showed significant improvement in imprint thickness variation, excessive thickness variations still exist due to inherent *ltv* of GaAs and InP substrates. For high-resolution features, the total thickness variation must be much smaller than the imprint feature height. For further investigations of imprinting on compound semiconductor wafers, it is necessary to have an imprint machine whose mechanical properties are fine-tuned and that can accommodate large surface variations of imprinting surfaces. Three research issues related to this problem are: a. Planarization of the top surface of the wafer, b. Use smaller templates for imprinting and c. wafer surface profile measurement tool and active template (or wafer) tip/tilting mechanism.

1. Introduction

Step and Flash Imprint Lithography (S-FIL)[1] is a low cost, high throughput, patterning technique with sub-50 nm resolution capability. It possesses important advantages over photolithography and other next generation lithography (NGL) techniques since it does not require expensive projection optics, advanced illumination sources, or specialized resist materials that are central to photolithography and NGL techniques. Imprint lithography techniques are essentially micromolding processes in which the topography of a template defines the patterns created on a substrate. Several imprint lithography techniques are being investigated as low cost alternatives for high-resolution patterning. Investigations by S-FIL group and others in the sub-100 nm regime indicate that the resolution is limited by pattern resolution of the template [2, 3, 4]. That is, the resolution of S-FIL appears to be only limited by the resolution of the template fabricating process.

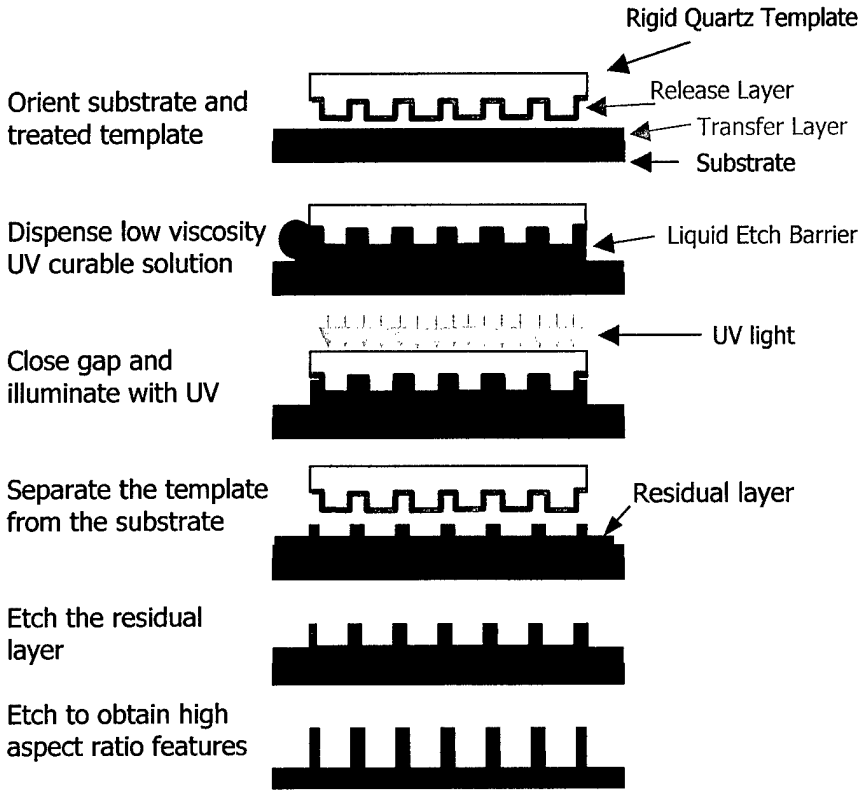

Figure 1. Step and Flash Imprint Lithography (low pressure, room temperature process).

S-FIL is an improved version of traditional micromolding based on a low-viscosity, UV-curable liquid etch barrier in conjunction with a bi-layer approach. This provides for a low pressure, room temperature process (Figure 1) that is:

- particularly suited for high-resolution layer-to-layer alignment [5],
- insensitive to pattern density variations, and
- capable of generating high aspect ratio, high-resolution features with high throughput.

S-FIL appears to compete quite well with the mainstream NGL technologies such as 157 nm photolithography (PL), electron projection lithography (EPL), and extreme ultraviolet lithography (EUV) techniques. The key competitive advantages of S-FIL over the other NGL techniques include:

- Sub-50 nm resolution
- Resolution = f(template); S-FIL is not a one node technology
- Significantly lower cost of ownership of S-FIL

Figure 2a shows top-down micrographs of 60, 40, 30 and 20 nm lines imprinted with a UV monomer [4]. The breakage in 20 nm lines has been contributed as a consequence of both the fidelity of the template and the high aspect ratio of the features. Figure 2b shows accurately repeatable patterning capability of S-FIL.

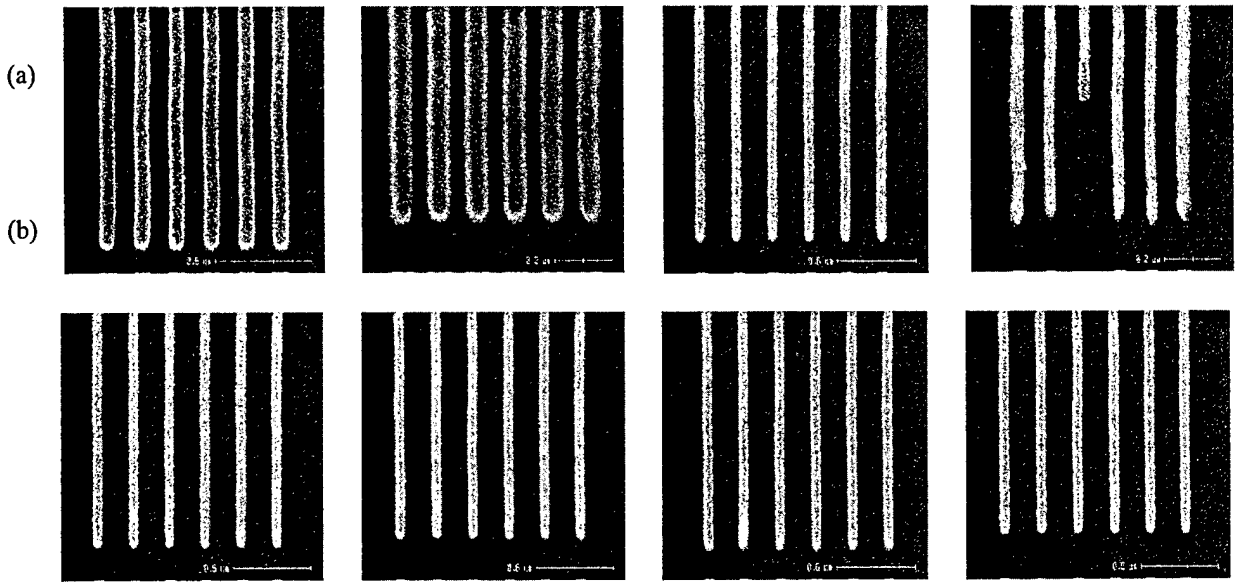

Figure 2. (a) Semi-dense 60, 40, 30 and 20 nm lines. (b) 30 nm printed lines from four different die (from D. J. Resnick et al., 2002 SPIE [4])

2. Compound Semiconductor Wafer Specifications

It has been known that the thickness variation of compound semiconductor wafers is not as well controlled as that of Si wafers. Typically, a tip-tilt mechanism can compensate for overall wafer tapers. Figure 3 provides a flatness specification of 4" GaAs wafers from a major wafer vendor (for a sampling group of >20K wafers). The local thickness variation (*ltv*) within imprinting area is the most critical parameter for imprint lithography processes since excessive *ltv* can cause large thickness variations in imprint layers. According to the vendor provided specifications, the *ltv* of GaAs wafers is excessive for

high-resolution imprinting. As addressed in the last section, various options that need to be researched are presented for imprinting on these wafers. Throughout this research, the issue of potential wafer breakage associated with imprinting has also been investigated.

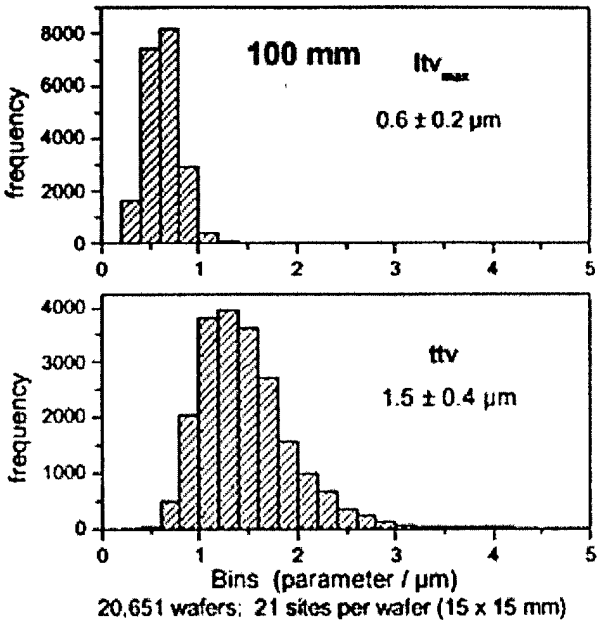

Figure 3. Local thickness variation (*ltv*) and total thickness variation (*ttv*) of 4" GaAs wafers (Source: Freiberger)

3. Proposed Tasks

Imprinting on compound semiconductor wafers such as GaAs and InP appears to be a challenging task. These wafers are much more fragile than Si wafers, especially when subjected to localized stresses. Such localized stresses can occur either via particles or large external loading during imprinting and separation. A proper support for substrates is also critical to generate satisfying imprint layers, where the thickness of imprint layer must be uniform and thin across the imprinted areas. Throughout this program, the following four issues have been investigated.

- *Investigate imprint force-thickness relationship*
- *Develop wafer chucks for imprint lithography processes*
- *Develop force measurement method and tool for S-FIL*
- *Gap height measurement scheme and tool*

4. Imprint Machines

For imprinting on compound semiconductor wafers, two imprint machines have been used during the reporting period. For the development of S-FIL process, a Multi-Imprint Machine (MIM), shown in Figure 4, has been developed at The University of Texas at Austin [6]. This machine can handle 8" wafers and generate imprint samples via step and repeat motions. The main purpose of this machine is to generate repeated samples on 8" Si wafers to investigate defect propagation issues associated with S-FIL [7]. Initially, this

machine was used to perform preliminary imprint tests on GaAs and InP wafers. However, due to a concern of cross-contamination associated with non-Si substrates, further tests were performed using UT Active Test Bed (ATB), shown also in Figure 4. This machine does not have a step-and-repeat capability. However, the tilting between the template and substrate can be actively controlled using three high-resolution actuators.

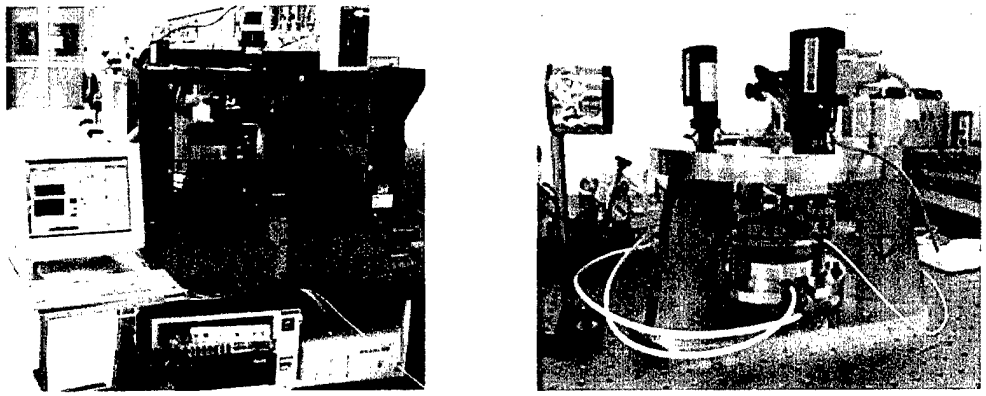

(a) (b)

Figure 4. Two imprint machines used for test: (a) UT Multi Imprint Machine (b) UT Active Test Bed

5. Task 1: Imprint Force-Thickness Relationship

As illustrated in the S-FIL process (Figure 1), imprinted layers need to be etched down to expose the bottom layer selectively. During this etching process, unless the imprint layer is thin and uniform, there can be a significant CD bias across imprint areas. In this section, analysis results about the relationship among imprint force, time and imprint layer thickness are presented.

a. Useful geometric and material variables

R, L: radius of a circular imprint, length of a square imprint

A: imprint size

μ: viscosity of liquid	(cp = 10^{-3} N s /m^2 = 10^{-21} N s/nm^2)
γ: surface tension	(dyne/cm = 10^{-5} N/cm = 10^{-12} N/*nm*)
V: volume of liquid	(*nl*)
h, h_i, h_f: gap height, initial, final	(*nm*)
t_f: time to close the gap	(s)

b. Fundamental models of template-fluid-substrate

A template and substrate form a small gap where an imprinting liquid is dispensed. The gap is closed to a certain value prior to an exposure step.

The template and substrate are assumed to be parallel initially and during the closing motion. Both square and circular templates are studied for cases of a completely filled gap and expanding liquid drops. Figure 5 illustrates two different cases.

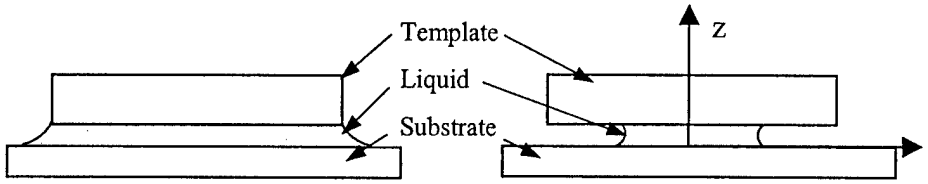

Figure 5. (a) Template-substrate with a gap completely filled and (b) gap with expanding liquid drop.

For the case of expanding drop(s), the volume of the dispensed liquid is equal to an imprint size multiplied with the final gap height. For template (and/or substrate) with features, the final gap height is selected as its "effective height[1]"[8].

c. Analytical solutions

Two basic equations form a non-compressible fluid model. First, the continuity equation is given as (using cylindrical coordinates)

$$\frac{1}{r}\frac{\partial}{\partial r}(ru_r) = -\frac{\partial u_z}{\partial z}. \tag{1}$$

Second, for a unit volume of liquid, the momentum equation is given as

$$\frac{\partial p}{\partial r} + \mu\frac{\partial^2 u_r}{\partial z^2} = 0. \tag{2}$$

Solving eqn. (2) with boundary conditions of $u_r(0) = 0$ and $u_r(h) = 0$, we have,

$$u_r(z) = \frac{1}{2\,\mu}\frac{dp}{dr}(hz - z^2). \tag{3}$$

Using eqn. (1) and eqn. (3), a solution for u_z (at $z = h$) is given as,

[1] "effective height" is a function of the depth of features (d), the smallest gap between the template and substrate (h, base layer height), and the density of features. For a completely filled template (50% feature), the effective height is approximately equal to $h+d/2$ [8].

$$u_z = \frac{h^3}{12\mu r}\left(\frac{\partial p}{\partial r} + r\frac{\partial^2 p}{\partial r^2}\right). \tag{4}$$

The u_z (at $z = h$) is equal to a template velocity. Then, the pressure distribution along radius becomes,

$$p(r) = \frac{3\mu(r^2 - R^2)}{h^3}\frac{dh}{dt} - \frac{2\gamma}{h} \tag{5}$$

where, the radius of meniscus is estimated as half of the gap height. It is expected that the radius of meniscus changes depending on the surface conditions of the template and substrate. Issues involved with a detail modeling of the radius of meniscus are not discussed here. It is important to note that the pressure distribution is a function of r^2 at eqn. (5).

The total imprinting force is the integral of eqn. (2) by $rdrd\theta$ over 0-R and 0-2π.

$$F = \int_0^{2\pi}\int_0^R p(r)rdrd\theta = 2\pi\left(-\frac{3\mu R^4}{4h^3}\frac{dh}{dt} - \frac{\gamma R^2}{h}\right) \tag{6}$$

Modeling for a square gap is more practical considering the real dicing geometry. However, considering the circular geometry of expanding drops, basic fluid modeling is more accurately represented for the case of a circular template. This is more applicable for the case of an expanding drop as compared to the completely filled case.

For a square template, the imprinting force becomes (using cartesian coordinates)

$$F = 0.422\frac{\mu L^4}{h^3}\frac{dh}{dt} - \frac{2\gamma L^2}{h}, \tag{7}$$

where, 0.422 is a "shape factor" for a square template and L^2 is the imprinting size [8, 9]. When $L^2 = \pi R^2$, forces at eqn. (6) and (7) differ by 6%. Following analyses are based on eqn. (6).

Gap closing time for a completely filled gap

For a completely filled gap, eqn. (6) simplifies into

$$F = -\frac{3\pi\mu R^4}{2h^3}\frac{dh}{dt}. \tag{8}$$

Then, the gap closing time is given as,

$$t_f = \frac{3\pi\mu R^4}{4F}\left(\frac{1}{h_f^2} - \frac{1}{h_i^2}\right). \tag{9}$$

Gap closing time for an expanding liquid drop

The volume of dispensed liquid is equal to that of an imprinting size multiplied with the final gap height ($V = Ah_f = L^2 h_f = \pi R^2 h_f$). From eqn. (6),

$$t_f = \frac{-3\mu V}{2\pi}\int_{hi}^{hf} \frac{dh}{h^3(h^2F + 2V\gamma)} \tag{10}$$

When the effect of a surface tension is negligible, eqn.(10) simplifies into

$$t_f = \frac{3\pi\mu R^4}{8F}\left(\frac{1}{h_f^2} - \frac{h_f^2}{h_i^4}\right) \tag{11}$$

Including the effect of a surface tension, the closed form solution for the gap closing time is given as,

$$t_f = \frac{3\mu}{16\pi\gamma^2}\left[2V\gamma\left(\frac{1}{h_f^2} - \frac{1}{h_i^2}\right) + F\ln\left(\frac{F + 2V\gamma/h_i^2}{F + 2V\gamma/h_f^2}\right)\right] \tag{12}$$

d. Comparison

Using eqn. (9) ~ (11), gap closing times are compared for the cases of a completely filled gap, expanding liquid drop without a surface tension, expanding liquid drop with a surface tension. Please note that the last case is the most suitable for real imprinting. It is necessary, however, to investigate the effect of a surface tension more thoroughly for a further improvement of the fluid modeling.

The first two cases can be analytically compared for their gap closing times while the third case is less straightforward even with a closed form solution. Issues related to the development of imprinting liquids and surface conditions of the template and substrate are presented later. Eqn. (13) shows the ratio between the first two cases. When $h_f < 0.1\ h_i$, the gap closing time for a completely filled gap is approximately twice that of an expanding drop without the effect of a surface tension.

$$\frac{t_f(case1)}{t_f(case1)} = \frac{2h_i^2}{h_i^2 + h_f^2} =\sim 2 \tag{13}$$

To compare the third case with others, two numerical examples are used. Geometric and material properties are selected as,

$A = \pi\, cm^2$ μ=1 cp = 10^{-3} N s /m^2 = 10^{-21} N s/nm^2

γ= 30 dyne/cm h_i = 1000 nm and h_f= 100 nm

Figure 6 compares gap closing times for the cases of imprinting forces of 10, 100 and 1000N. It is clearly noticeable that the case of an expanding liquid is more practical as compared to others where the template and substrate cannot handle high imprint pressures, especially for imprint lithography processes.

Instead of a single drop of liquid, multiple small drops of fluid can be dispensed on imprinting sites. The total volume of multiple drops of liquid is equal to that of the case of a single drop. The total imprinting force, F_t, for an n-drop case, is given as $F_t = n\, F_n$. For n-drop of a volume $V_n = V/n$, total imprinting force, F_t, is given as,

$$F_t = nF_n = n\frac{3\mu A_n^2}{8\pi t_f}\left(\frac{1}{h_f^2} - \frac{h_f^2}{h_i^4}\right) = n\frac{3\mu (A/n)^2}{8\pi t_f}\left(\frac{1}{h_f^2} - \frac{h_f^2}{h_i^4}\right)$$
$$= \frac{1}{n}\frac{3\mu A^2}{8\pi t_f}\left(\frac{1}{h_f^2} - \frac{h_f^2}{h_i^4}\right) = \frac{F_s}{n} \qquad (14)$$

where, F_s is the imprinting force for the case of a single drop. Here, for the purpose of simplicity, identical n drops are used. Then, for a fixed gap closing time, imprinting force decreases by a factor of n. Or, if the imprinting force is fixed, the gap closing time decreases by a factor of n. This is solely due to the fact that the imprinting force is a function of area square [10].

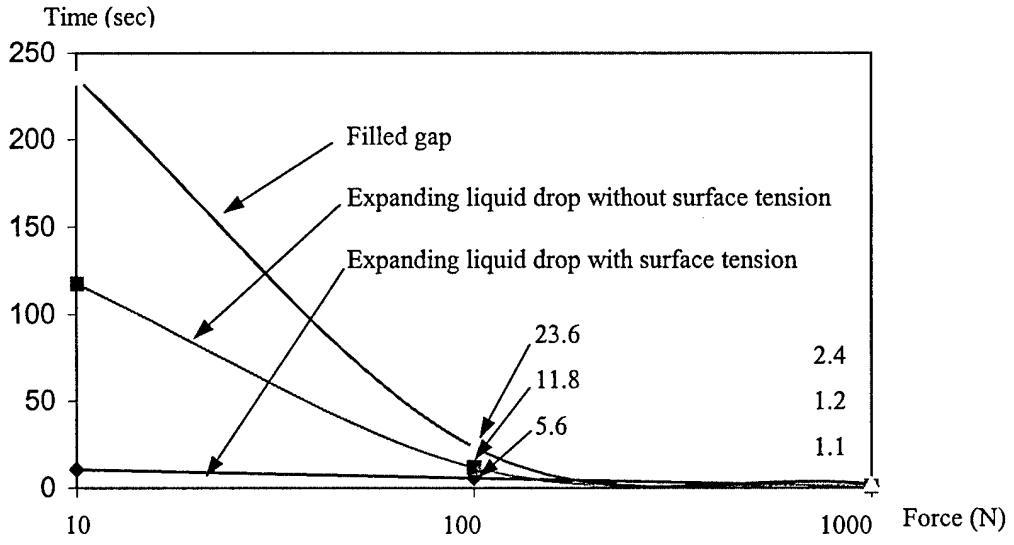

Figure 6. Gap closing times for three cases.

When the surface tension is included into the model, the benefit of n-drop does not explicitly appear in eqn. (12) due to the absence of a closed form solution of imprinting forces. Therefore, numerical cases are presented here. In order to maintain the total imprinting force constant, the imprinting force at each drop is given as F/n. Gap closing times are computed for the cases of two-drop and ten-drop. As shown in Figure 7, it is clear that an n-drop method is very effective this case.

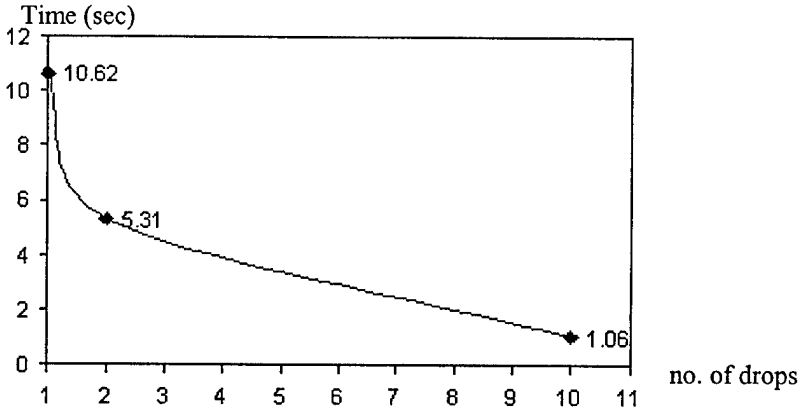

Figure 7. Gap closing time from 1μm to 100nm for 1, 2, and 10 drops with F = 10N.

6. Task 2: Wafer Chuck Design

For imprint processes, it is important to provide a uniform support at the backside of a wafer. Otherwise, excessive wafer deformations can occur and eventually mechanical failure can result, especially for highly localized deformations such as those caused by backside particles. In order to minimize the back-side particle problem, the ratio of contact surface with respect to wafer surface needs to be maintained low enough without causing large local stresses in wafers. For Si wafers, typically less than 10% of the wafer back surface contacts the chuck surface. However, it is relatively unknown if such a low contact ratio may lead to excessively localized stresses for compound semiconductor wafers.

a. Top surface profiles

Surface deformations of wafers have been analyzed for two types of wafer chucks with pin type and fine grooved top surface profiles. Figure 8 shows top surface geometries of

two types of chucks and graphical FEM results of the wafer top surface deformations. The imprinting pressure applied from the top surface of the wafer was given as a uniform pressure. The vacuum force was modeled as a uniform pressure and applied only on the portion of the back side of the wafer that does not contact with the chuck top surface. Chuck top surfaces have 0.5 mm pin or wall with a pitch of 2 mm. The chuck bottom surfaces of models shown in Figure 8 were constrained in all six axes. Therefore, the bending deformation of the wafer chuck was not included in these models. FEM analyses showed ~25 nm and ~10 nm deflections with 350 micron thick GaAs wafers for the pin type chuck and fine-grooved chuck respectively. The total pressure of vacuum holding and imprinting forces was modeled as 120 kPa.

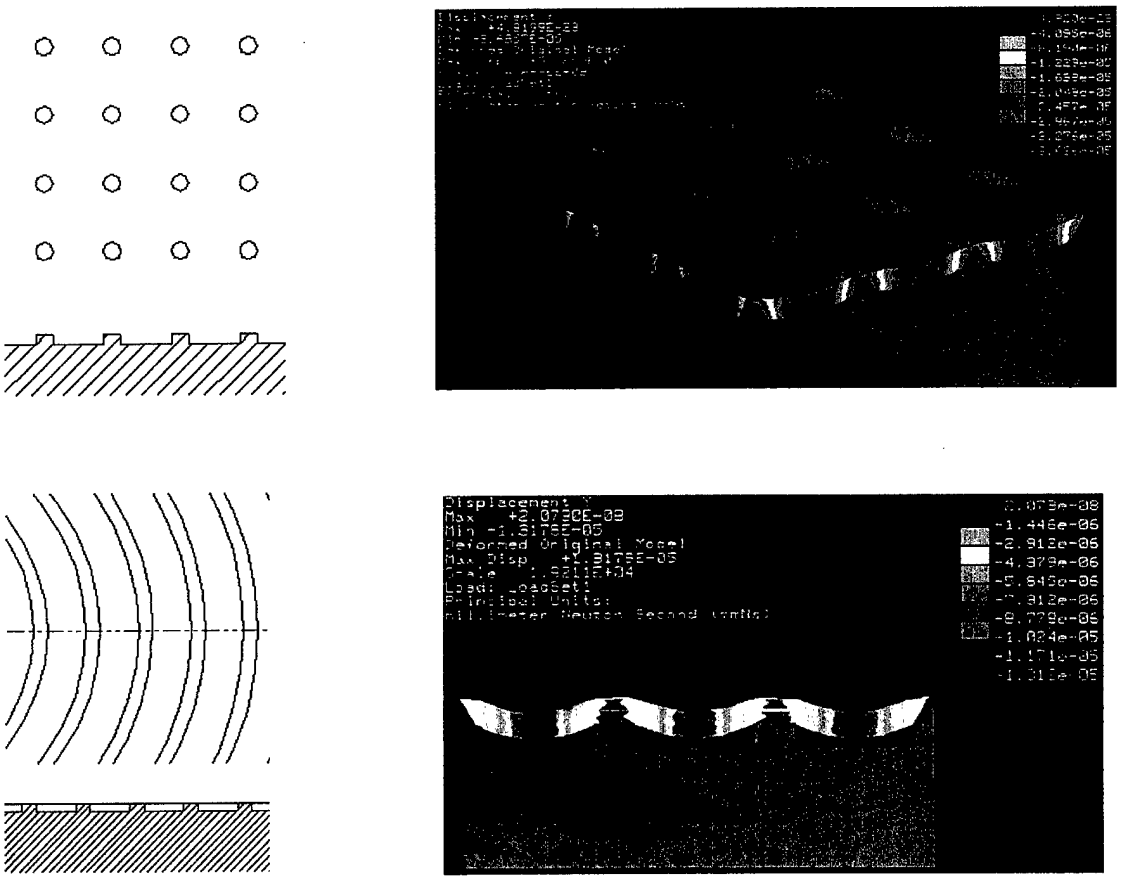

Figure 8. Pin type (top) and fine grooved (bottom) wafer chuck patterns. FEM analyses showed ~25 nm and ~10 nm deflection using 350micron thick GaAs wafer. Both the vacuum and imprinting forces were applied (total 120 kPa).

b. Prototype wafer chucks

The wafer surface deformations under imprinting and vacuum pressures have been analyzed with respect to the interface of the chuck and wafer. However, the overall surface variation of a wafer is a combination of deformations due to the interface of the chuck and wafer, and bending deformations of the wafer chuck itself under external forces. In order to model the surface variation due to the bending, additional chuck geometric parameters need to be defined, such as its diameter and thickness. Further, detailed mounting mechanisms of the chuck to XY stages must be defined in order to assign boundary conditions properly.

Figure 9 shows two fine grooved vacuum chucks. The universal chuck has divided vacuum areas to accommodate 2, 3, 4, 6, and 8" wafers. Its thickness was selected to be as 20 mm based on thorough FEM analyses with SiC, and it has a web structure in order to increase the ratio of bending stiffness vs. weight. Two prototype wafer chucks were fabricated from heat-treated stainless steel.

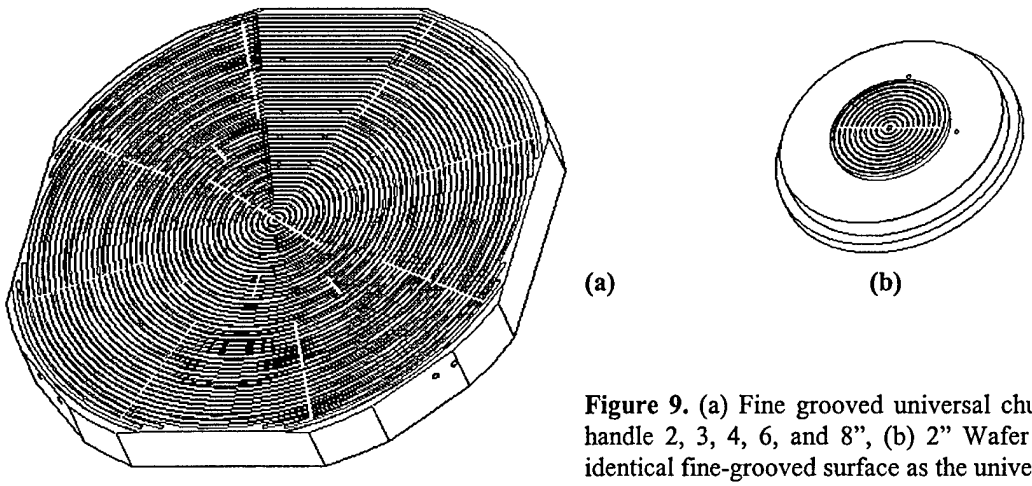

Figure 9. (a) Fine grooved universal chuck that can handle 2, 3, 4, 6, and 8", (b) 2" Wafer chuck with identical fine-grooved surface as the universal chuck

c. Assembly methods for wafer chucks

Wafers chuck top surfaces can be optically polished to better than 2 micro-inch ($<\lambda/10$). However, wafer chucks can be excessively distorted depending on assembly methods with respect to their mating surfaces or fixtures. As compared to other lithography processes, imprint lithography processes requires the wafer chuck to be fixed against both

pulling and pushing forces. Therefore, it is important to properly fix wafer chucks to an XY stage platform without distorting the top surface.

For the smaller wafer chuck, three pre-loaded kinematic fixture were used to hold the chuck without sacrificing bending stiffness significantly (15mm thick heat treated stainless steel body). Figure 10 illustrates the pre-loaded kinematic fixture of the smaller chuck on a wafer chuck stage.

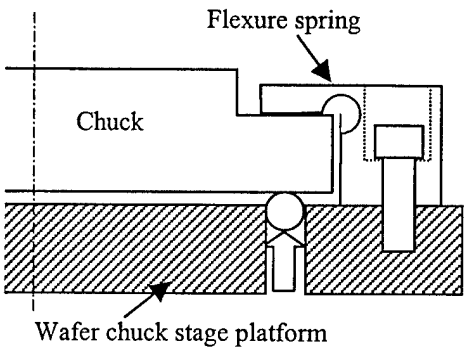

Figure 10. Pre-loaded kinematic fixture for the smaller wafer chuck (three locations)

For the universal wafer chuck, it is not practical to implement such a kinematic fixtures. FEM analyses showed that imprinting forces on substrates outside a triangle formed by the three fixing points cause a large tilting of the wafer chuck surface, mainly due to bending of the chuck itself. The thickness of the chuck cannot be beyond a reasonable height due to potential machine interfacing problems such as interference, Abbe error and carriage weight limit. After a thorough FEM analysis, 20 mm SiC body with web back structure was selected for the chuck. Three large circular vacuum areas were made at the backside of the chuck. A mating surface that support the wafer chuck needs to be polished in order to maintain a vacuum seal. By using large vacuum supports through the back surface of the chuck, local deformation (as compared to a bolting-down method) and large bending deformation (as compared to simple kinematic fixture) can be avoided. Figure 11 shows the web structure and three vacuum areas for the wafer chuck fixture developed by Molecular Imprints, Inc in collaboration with M cubed Technologies, Inc, who specializes in the area of high-end wafer chuck manufacturing.

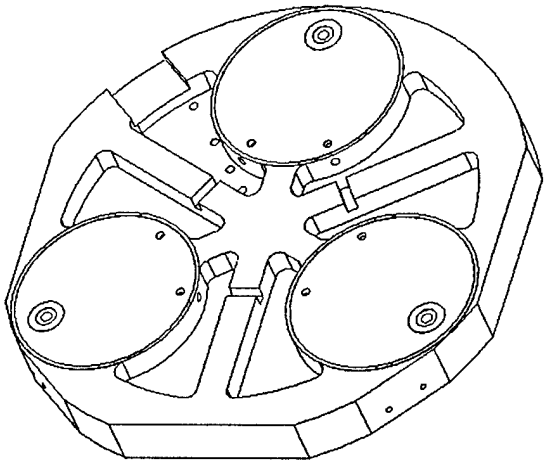

Figure 11. Web structure of the wafer chuck back side. Three vacuum areas are used to hold the chuck in place during both imprint and separation

Two wafer chucks were installed on the two UT imprint machines as shown in Figure 12. Prior to fabricating SiC wafer chucks, an 8" heat treated stainless steel chuck was machined and polished in order to assess the feasibility of the suggested design. Step and repeat imprints on 8" Si wafers indicated no excessive bending or surface variations on the 8" universal wafer chuck. Individual vacuum holding for various wafer sizes also showed no vacuum loss between the substrate and chuck top surface.

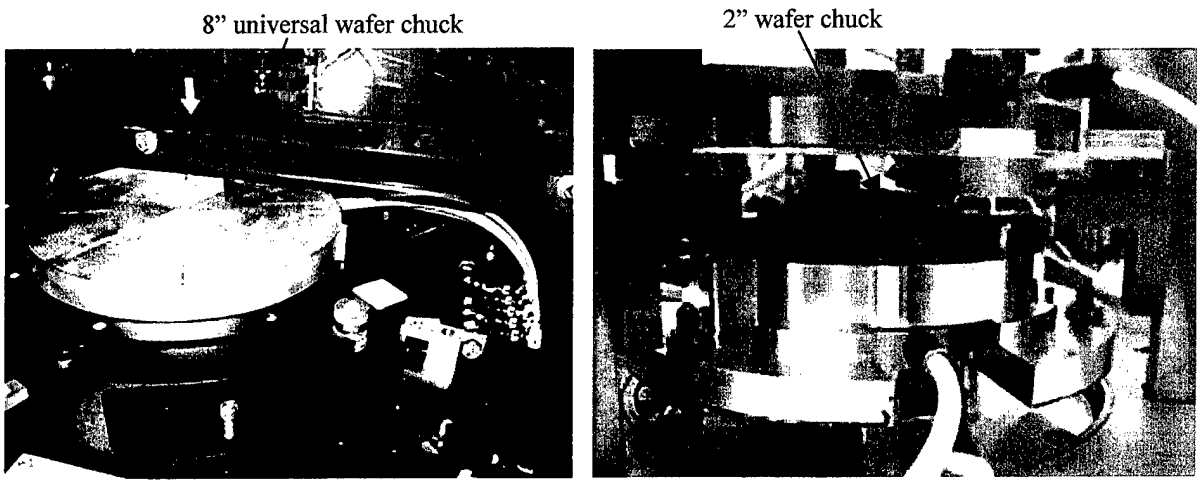

Figure 12. (a) Universal fine-grooved wafer chuck is installed on UT MIM with five independent vacuum controls. (b) Two inch fine grooved wafer chuck is installed on the wafer stage of UT ATB.

7. Task 3: Force Measurement Method and Tool

It is important to measure the imprinting and separation forces for two purposes: safety limits and real time force control feedback. In either case, it is important to minimize any additional compliance induced to imprint machines originated from the deflection at the load cells. Excessive compliance at load cells can induce template lateral displacement during imprinting and separation. Typically, strain gage type load cells have more than 1 μm deflection for 10 N when their sensitive range is 0 to 100 N. As compared to the strain gage load cells, piezo load cells have mush better stiffness characteristics, for which compliance is less than 10 nm/10 N in the same sensitive range. Therefore, three piezo dynamic load cells (PCB Inc, Model number 208C02) were selected for the purpose of imprint and separation force measurement. The piezo load cell does not require an external power source, which makes it less exposed to outside noise. However, the piezo generating voltage will dissipate soon after the gap closing motion stops (in the range of seconds) due to electrical isolation imperfections in realistic applications. Since

the actual gap closing motion and separation occurs much faster than one second, such losses in signal should not hinder the load cell from being used for S-FIL processes. However, for high pressure imprinting processes, it is not practical to use such dynamic load cells since the gap closing between the template and substrate takes much longer as compared to that of S-FIL.

In order to measure the forces, three load cells are used and they are distributed symmetrically about the template. Symmetrical configuration ensures equal deflections at all three load cells, and in the case of small differences in deflections, the high stiffness of the piezo load cell will prevent the template from moving laterally with respect to the substrate. Figure 13 shows the load cell installed between a high resolution imprint actuator and flexure ring of ATB that selectively constrains the template. Tests showed that the load cell reading is sensitive enough so that the template and substrate relative tilting can be qualified by simply measuring the differences among the three force outputs.

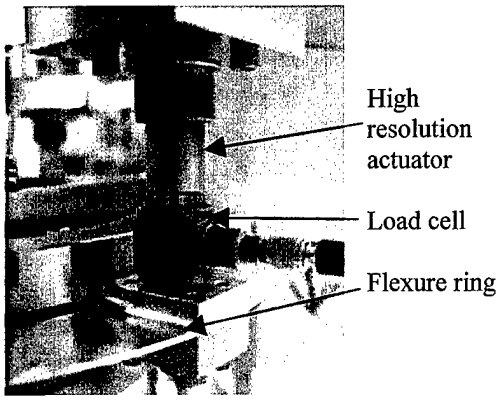

Figure 13. Piezo load cell attached between the actuator and flexure ring of ATB

8. Task 4: Gap Height Measurement Scheme and Tool

a. FFT based spectrometer

For the gap measurement, a broadband spectrometer that collects light across 400 – 800 nm bandwidth is used. Traditional gap height and film thickness measurements are based on curve fitting methods that map through the collected data (intensity vs wavelength, λ) to fit them with analytically formulated curves. However, such curve fitting processes are not practical for the purpose of a fast gap measurement. Gap height data at three or more points can be used to compute the relative distance and orientation between the template and substrate.

Recently, a new computationally efficient algorithm for the gap measurement has been developed for imprint lithography processes by the author of this report and others [10]. Figure 14 shows the scheme. Based on the observation of intensity being a function of n/λ, where n is the reflective index, a Fast Fourier Transform algorithm that computes

a frequency equivalent number (no. of oscillations within the band of 1/800 and 1/400) of the intensity signal in the $w = 1/\lambda$ domain has been developed. Recent test shows that the gap between template and substrate can be computed up to 13 Hz. The measurement rate, at this moment, is not limited by the computation algorithm but by the data transfer rate from the spectrometer card to the main computer. Oceanoptics, Inc., who supplied the spectrometer unit, is currently working on improving the transfer rate significantly. It is expected that without any major modification to the algorithm, much faster gap measurement can be achieved as a future work.

When the gap between the template and substrate goes approximately below 250 nm, the number of oscillations becomes less than one. In such a case, the exact gap is difficult to estimate since the sensitivity in the FFT algorithm decreases. Therefore, an alternative algorithm needs to be developed for smaller gaps than ~250 nm. Presented in Section 8b is the process description for cases when multiple oscillations exist within the band of the wave numbers and when less then one full oscillation exists.

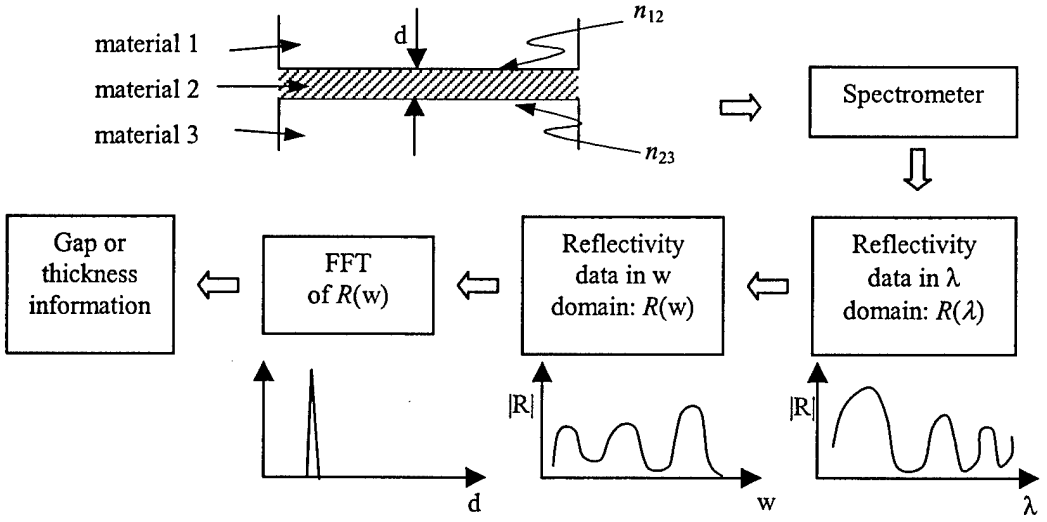

Figure 14. Process of the thickness, or gap, measurement technique via FFT

Experiments were performed with two types of gaps: spin coated film on Si wafers and air or water gap between the template and substrate. Both gaps (or films) were above 500 nm for the test. Measurement data using the developed algorithm showed promising accuracy as compared to data from two types of other film thickness measurement tools: Tencor Profilometer and Nanospec 4100.

Implementation of this algorithm into more efficient programming languages and development of a multi-probe unit will be one of the future issues associated with this task.

b. Description of FFT based of gap measurement

1. Collect reflective data using a broad band spectrometer
2. Data generated is in λ domain. The digitized data is not evenly spaced in the λ domain. However, a calibration of a spectrometer can provide an accurate wavelength for the corresponding spectrometer pixel address.
3. The oscillation of the reflectivity is the period in the $1/\lambda$ domain. Convert the digitized data $R(\lambda)$ into R(w), where $w = 1/\lambda$ (It is assumes that n is constant within the broadband. Otherwise, convert the digitized data into R(nw)).
4. If multiple oscillations exist between $1/\lambda_{max}$ and $1/\lambda_{min}$:
    - FFT analysis using a window leads to a single peak (say, p_1). The thickness of the measuring object is $p_1/[(1/\lambda_{min}-1/\lambda_{max})*2n*m]$. Here, m is the magnification factor in FFT (ratio of FFT data vs real data).
    - Windowing will improve the accuracy.
    - Adding zeros to the end of the data will improve the resolution of the FFT analysis.
5. If less than a full oscillation exists between $1/\lambda_{max}$ and $1/\lambda_{min}$:
    - FFT for this case may yield large error due to the ill-conditioned data.
    - Alternatively, find a point where the reflectivity is max or min.
    - One of the important aspects of the reflectivity data is that, at $w = 0$ (or $\lambda =$ infinite), **dR/dw= 0** and R is at its local max.
    - From 0 to $1/\lambda_{max}$, a smaller portion of an oscillation exists as compared to that of $1/\lambda_{max}$ and $1/\lambda_{min}$ when $1/\lambda_{min} >= 2/\lambda_{max}$
    - Find w_1, where $\mathbf{R(w_1) = min}$, or **max** ($w_{min} < w < w_{max}$)
    - Depending on the size of the portion of the oscillation within ($w_{min} < w < w_{max}$), different computation algorithm are used (under development).

- The limit of measurable thickness of a thin film can be as low as the one that generates only 1/4 of oscillation within (1/800 nm – 1/400 nm). For this case, the w_1 will be at 1/400 nm, which corresponds to 0.5 in FFT peak location with dw = 1/400. Therefore, $d = p_1/[(1/\lambda_{min}-1/\lambda_{max})*2n*m] = 0.5*400/3 = 67$ nm. Here, m = 1 and n =1.5 Also, a spectrometer with a 200 nm – 800 nm range is readily available. For this wave range, at least 3/4 oscillation is needed. For this case, the minimum thickness will be d = 0.5*200/3 = 33 nm.

9. Imprint Samples

a. Test wafer preparation

GaAs and InP wafers were spin-coated with a photo resist and baked in order to make wafer surface energy high enough for imprinting. Wafers were coated with HR100 at 3500 prm for 60 sec and baked on a hot plate for 1min at 120 °C. After the wafers were UV blank exposed for 1 min, they were hard-baked on a hot plate for 5 min at 120 °C (the thickness of the photo resist was approximately 1180nm).

b. Imprint images on GaAs and InP

In order to test for potential wafer failure during the imprint and separation, imprints have been performed both at the center of the wafers and also over the edge of the wafers in order to simulate partial die imprints. Neither imprinting force (up to 30 lb) nor separation caused wafer breakage during the test, except for two occasions; a large particle on the chuck caused a wafer breakage during vacuum suction prior to imprinting, and a prior scratch on the wafer caused a visible crack propagating along a crystallographic orientation of an InP wafer (Figure 15). It is expected that such cases of concentrated stresses can be prevented in a practical implementation with particle detection and proper wafer loading schemes.

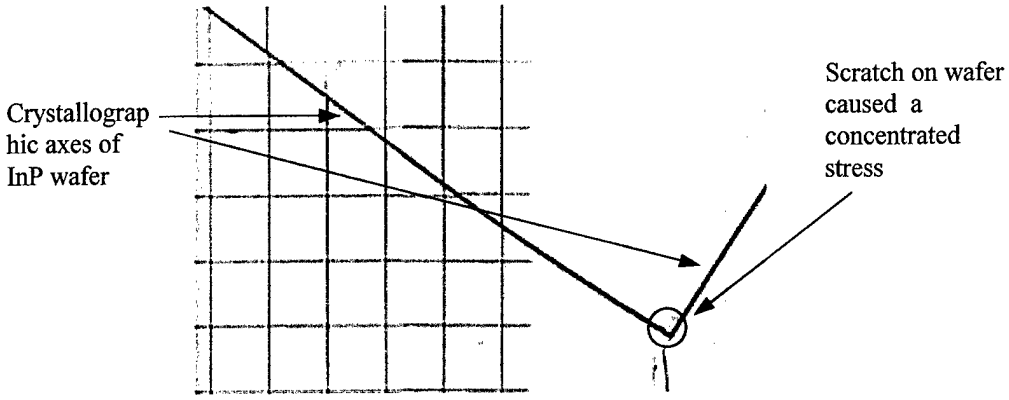

Figure 15. Crack on InP along its crystallographic orientation

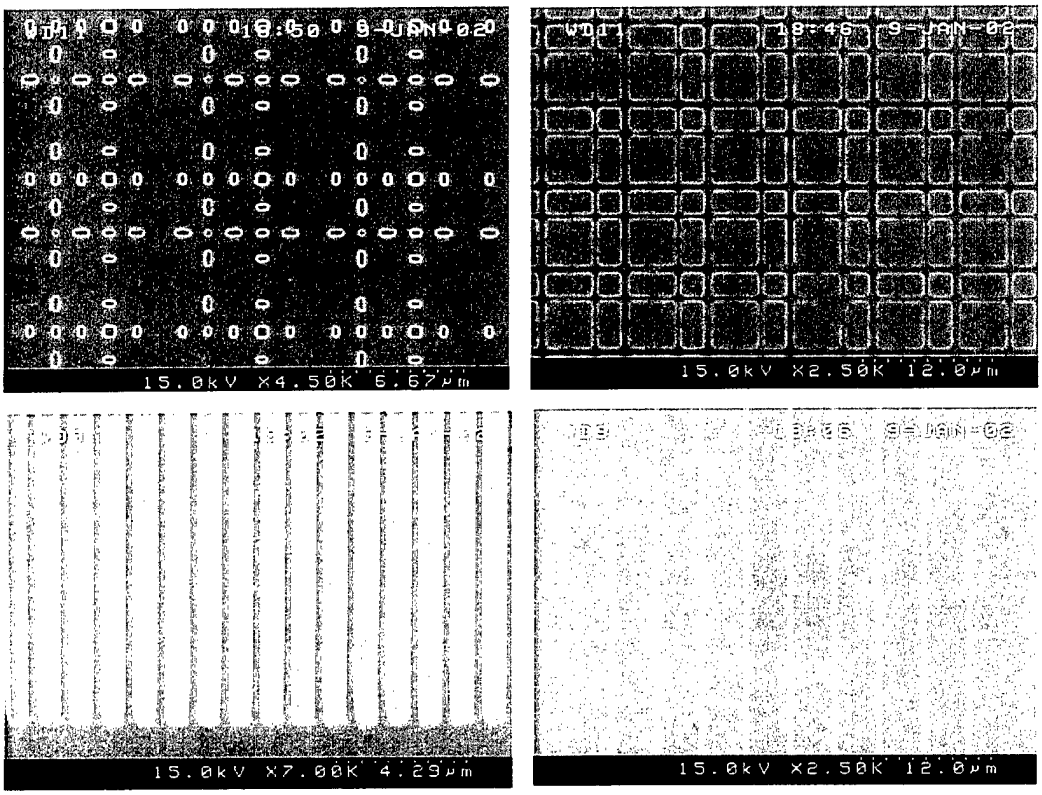

Figure 16. SEM images of imprints on GaAs wafer; top two images show successful patterning of bit failure test patterns, bottom left shows 650 nm and bottom right shows 200 nm lines.

Figure 16 shows SEM images of imprinted layer on GaAs and InP wafers. Imprint area was 25 mm by 25 mm with an approximately 12% patterned area. The template used for imprints on compound semiconductor wafers has smallest features of 200nm. As shown in Figure 2 earlier, it is strongly believed that the resolution of the imprint itself can be as small as tens of nano meters.

c. Imprint thickness variation

In section 2, the local thickness variation (*ltv*) of 4 inch GaAs wafers (Freiberger) was presented. It is expected that such a large thickness variation of compound semiconductor wafers will cause a significant difficulty in generating uniform imprinted layers, especially for large templates. Figure 17 illustrates potential problems associated with non-uniform imprint layer caused by either the mis-alignment between the template and substrate or large thickness variation of the substrate.

Figure 18 shows a plot of a thickness measurement of an imprinted layer on an InP wafer. Several other imprints also showed similar thickness variations. Multiple

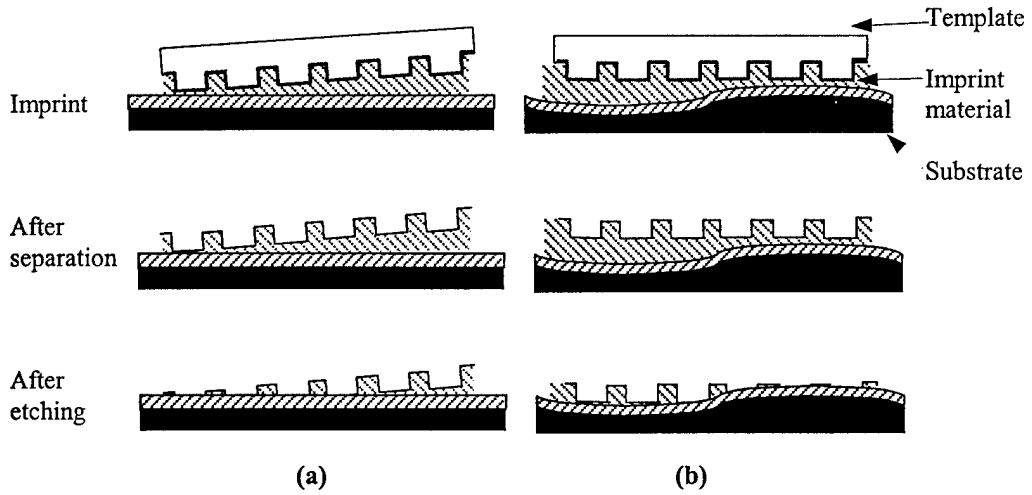

Figure 17. Undesirable imprint layers that can cause partial loss of patterns after etching: (a) mis-aligned template-substrate and (b) excessively waved substrate surface

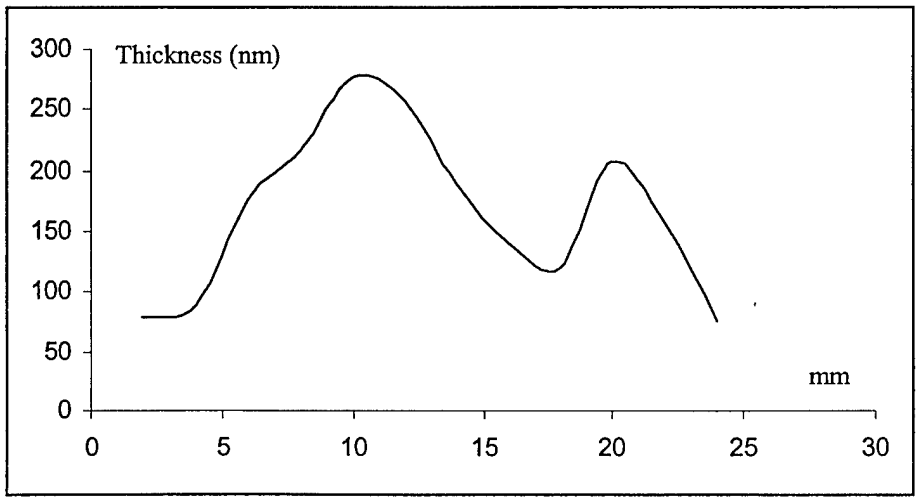

Figure 18. Thickness variation of imprinted layer across 25 mm on an InP wafer with ~1.180 μm HR 100 spun photo resist layer.

sources of potential problems are expected to cause such a large thickness variation in conjunction with the large *ltv* of compound semiconductor wafers. A major source is the current template holding mechanism, where only the small edge of the template is supported during the imprinting. Other sources include problems associated with imprinting fluid management and compliant, thick photo resist layer. In order to solve this problem, three suggestions are presented at the end of this report as future work.

10. Conclusions

Repeated imprint tests with up to 30 psi pressure on compound semiconductor wafers were performed. Except for the cases of large particles that induced localized stress on substrates, imprinted wafers did not show any macro-scale wafer failure during the test. However, it is not known if micro-scale damages on the wafers are present at this moment. In order to generate a uniform and thin imprinting layer, the wafers must be supported uniformly and the surface contact ratio at the wafer-chuck interface needs to be low to minimize the back side particle problem. Also, a low contact ratio can induce not only excessive surface variations but also mechanical failure to the wafers due to localized stresses. Two wafer chucks that have fine-grooved surface with ~20% contact area were fabricated; 2" wafer chuck and a universal wafer chuck for 2, 3, 4, 6, and 8". Imprint test with a prototype universal chuck showed satisfying results. A wafer chuck vendor is fabricating a SiC wafer chuck with an identical design.

The force-time-thickness relationship has been analyzed. The significant differences between a fully filled gap and fluid expanding gap, and between a single drop and separated n-drop cases were presented.

During the imprint processes, it is important to monitor both the imprint force and gap between the template and substrate, not only to prevent accidental template-substrate interference but also to provide feedback for either position or force control. Further, it is expected that potential mis-matching between force and gap data can be used as an indicator to detect the presence of a large particle at the template and substrate interface. The selection of load cells and assembly methods were presented in this report. Experiments showed satisfying results with the selected load cells. For a fast gap measurement, an FFT algorithm using intensity data from a broadband spectrometer was

presented. It is believed that real-time gap information will be significantly beneficial to monitor and control the relative orientation between the template and substrate in imprint lithography processes.

11. Future Work

During the proposed research period, the main tasks have been accomplished. Using two existing UT imprint machines, with appropriate modifications and improvements, imprint tests on compound semiconductor wafers have been performed. Future work associated with tasks presented in this reports are itemized in this section.

a. Experimental imprint machine development

It is essential to allocate an experiment tool for the purpose of unique imprinting characteristics associated with compound semiconductor wafers. As reported in the first quarter report, UT MIM has significant compliances in its imprinting mechanism. UV curing imprint lithography techniques are suitable for high resolution alignment since the low imprint force and no temperature variation during the process will not cause template and substrate deformation. However, in order to keep the template and substrate aligned during the measurement and imprinting, imprinting mechanism needs to possess high stiffness. In such a case, the template will induce a near-impact loading to the substrate during the gap closing motion. Therefore, it is necessary to develop a unique imprint machine that has a well-controlled machine stiffness to investigate the effect of impact forces during imprinting and separating on compound semiconductor wafers

b. Implementation of a numerical algorithm to expand the gap measurement lower limit beyond 250 nm

For larger gaps, experiments showed promising results using the FFT algorithm. However, it is essential to expand the lower limit of the scheme beyond the cases where only less than a full oscillation is present within the light bandwidth. It is possible to use a larger bandwidth in order to bring down the lower limit. However, using any significantly short wavelength is not practical due to the presence of UV monomer for imprinting. It is

necessary to implement the case of smaller gap into numerically efficient programming and to verify its practical accuracy.

c. Improvement for imprint thickness variation control

i. Template holding mechanism development

Templates used for imprinting at S-FIL are made of ¼" quartz. The template fabrication process is analogous to the current industry standard for the fabrication of phase-shift high-resolution photo masks. Unlike photolithography processes, templates contact substrates indirectly in the presence of fluid, which also induces a significant pressure distribution at the interface. Therefore, it is important to support the template rigidly so that during the imprinting and separation, no mechanical failure occurs. However, the UV exposure for S-FIL process requires most of the backside of the template to be open for the exposing light. Current UT machines support templates through only small edges of backsides and additional supports come from eight setscrews from side surfaces of templates. It has been found (from both repeat experiment and FEM analyses) that such a holding mechanism causes significant template distortion in both surface and bending. Therefore, it is important to develop a new scheme to provide secure and uniform support to the template while letting the UV exposure light pass through the template.

ii. Planarization scheme and process development for compound semiconductor imprinting

When the substrate itself possesses significant large surface variation, it is necessary to planarize the imprinting area, especially for high-resolution imprinting. Chemical-Mechanical Polishing (CMP) has been used for existing photolithography processes. However, the CMP process is expensive and only limited surface improvement can be made. It is also an abrasive process which may be unsuitable for compound semiconductor wafers. Since the requirement of the surface flatness is much tighter for imprinting processes, it is necessary to implement a planarization scheme. During the process development of S-FIL, a planarization was suggested by using a blank template to imprint on uneven surface to generate near perfect flat surface (with different etch-selective imprinting material as compared to that of imprint layer). Imprinting will be

performed on the flat imprinted layer. In order to perform such a planarization, it is necessary to orient the blank template in a selected tilting configuration, which does not necessarily coincide with the average plane of the local area of the substrate. It is expected that such a task requires actively controllable tip/tilt stages for the template (or for the wafer) along with real-time gap measurement.

iii. Smaller imprinting area with active tip/tilting

Depending on surface thickness variation (absolute magnitude of the variation and number of waves), it is expected that near uniform imprinting layer can be generated by selecting the size of imprints small enough and, during step-and-repeat, orienting the substrate and template in a die-to-die manner. It is also essential to have a real-time gap measurement tool for a high throughput.

d. Effect of the thickness and compliance of spin-coated layer below the imprinted layer

Another interesting area of investigation will be the effect of the spin-coated layer on which the imprinting layer will be formed. When the underlying layer is thick and compliant, it is expected that the large deformation of the layer will affect the thickness variation of the imprinting layer. When the underlying layer is too thick, one of the potential difficulties will be the development of a well-controlled etching process.

References

1. M. Colburn, *et al.*, 1999, "Step and Flash Imprint Lithography: An alternative approach to high resolution patterning." Proc. SPIE Vol. 3676, 379-389, 1999.
2. S. Y. Chou, *et al.*, *Nanoimprint lithography.* J. Vac. Sci. Tech. B, 1996. **14**(6): p. 4129
3. Xia, Y. and G.M. Whitesides, *Soft Lithography.* Angew. Chem. Int. Ed. Engl., 1998. **37**: p. 550.
4. D. J. Resnick et al., "High Resolution Templates for Step and Flash Imprint Lithography", SPIE: Emerging Lithographic Technologies V. 2002, 4688-21.

5. B. J. Choi, *et al.*, "Layer-to-Layer Alignment for Step and Flash Imprint Lithography". in Proc. SPIE: Emerging Lithographic Technologies V. 2001.
6. B. J. Choi, *et al.*, 2000, "Design of Template Alignment Stages for Step & Flash Imprint Lithography", J. American Society for Precision Engineering.
7. T. Bailey, *et al.*, "Step and Flash Imprint Lithography: Template Surface Treatment and Defect Analysis." *J. Vac. Sci. Technol. B.* 18(6), 3572-3577 (2000)
8. Freeland, A. C. "Mathematical modeling of the dynamics and production of biosensors." Ph.D. dissertation, The University of Texas at Austin, 2000.
9. Hays, D.F. 1962. Squeeze films for rectangular plates. ASME Paper No. 62-Lub-S.
10. Colburn, M.E., Step and Flash Imprint Lithography: A Low-Pressure, Room-Temperature Nanoimprint Lithography. Department of Chemical Engineering; Ph.D. Thesis. 2001, Austin, TX: The University of Texas at Austin.